Submitted to Nuclear Physics B

UCRL-19427
Preprint

THE $K\pi$ SYSTEM IN THE CHANNEL $K^+\pi^-\Delta^{++}$ AT 9 GeV/c

C. Fu, A. Firestone, G. Goldhaber, and G. H. Trilling

December 4, 1969

AEC Contract No. W-7405-eng-48

LAWRENCE RADIATION LABORATORY
UNIVERSITY of CALIFORNIA BERKELEY

DISCLAIMER

UCRL-19427

THE $K\pi$ SYSTEM IN THE CHANNEL $K^+\pi^-\Delta^{++}$ AT 9 GeV/c[†]

C. Fu, A. Firestone, G. Goldhaber, and G. H. Trilling

Department of Physics and Lawrence Radiation Laboratory
University of California, Berkeley, California 94720

December 4, 1969

Abstract: The study of the $K\pi$ system in the channel $K^+\pi^-\Delta^{++}$ is complicated by the presence of the broad low-mass $\Delta^{++}\pi^-$ enhancement centered near 1580 MeV. A cut which removes this effect reveals a break in the t' distribution at $|t'| \approx 0.05$ $(GeV/c)^2$, with a very steep forward peak of slope $a = 23.6\pm5.2$ $(GeV/c)^{-2}$ for $|t'| < 0.05$ $(GeV/c)^2$ and a slope of $a = 9.5\pm2.0$ $(GeV/c)^{-2}$ for $|t'| \geq 0.05$ $(GeV/c)^2$. We associate this forward peak with a single-pion-exchange mechanism. A small enhancement at $M(K^+\pi^-) \approx 1100$ MeV is observed in a t' region dominated by non-pion-exchange mechanisms.

[†]Work supported by the U. S. Atomic Energy Commission.

1. Introduction

There has been rather extensive discussion of states that may contribute to the Kπ mass spectrum in the region from K^*_{890} to K^*_{1420}. Specifically there have been the suggestions of a wide s-wave Kπ state near 1100 MeV[1]) and a p-wave Kπ state near the K^*_{1420}[2]), both based on interference effects with each of the two principal adjacent K^*'s. Furthermore, studies of the Kπ mass spectra in a number of different experiments have observed some evidence for several small mass peaks between the two principal K^*'s[3]). This paper presents the results of a study of the production mechanisms of the reaction $K^+p \to K^+\pi^-\Delta^{++}_{1236}$ as a function both of Kπ mass and of t'[4]). We shall use the symbol Δ^{++} to refer to the Δ^{++}_{1236} resonance. The study is based on a sample of 7552 events of the reaction $K^+p \to K^+\pi^-\pi^+p$ at 9 GeV/c from which we select 2954 events in the Δ^{++} band [1.12 GeV ≦ $M(p\pi^+)$ < 1.32 GeV] and with $|t'| < 10$ $(GeV/c)^2$.† This latter cut eliminates a small nonperipheral background.

†We use the symbol t', defined as $t' = t - t_m$, where t is the square of the four-momentum transfer from the incident K^+ to the outgoing $K^+\pi^-$ system, and t_m corresponds to the Chew-Low boundary adjacent to the peripheral region.

The main conclusion we draw from our study is that pion exchange is dominant only in a very small forward region, $|t'| < 0.05$ $(GeV/c)^2$, and that even in this region the low-mass $\Delta^{++}\pi^-$ enhancement contributes to asymmetry in the Kπ decay system. Hence any quantitative conclusions about a Kπ s-wave state--which may well be present--must be evaluated with due concern for these limitations. More specifically, in the study of the above sample we make the following experimental observations:

(1) The low Kπ mass region [$M(K^+\pi^-) < 1.54$ GeV] is dominated by $K^*_{890}\Delta^{++}$ and $K^*_{1420}\Delta^{++}$ double resonance production. The high Kπ mass region [$M(K^+\pi^-) \geqq$

1.54 GeV] is associated with a low-mass $\Delta^{++}\pi^-$ enhancement with $M(\Delta^{++}\pi^-) \approx 1.58$ GeV, and with $\Gamma(\Delta^{++}\pi^-) \approx 0.35$ GeV. This well-known enhancement is strongly correlated with forward θ values, where θ is the $K\pi$ scattering angle in the $K^+\pi^-$ center-of-mass system (Jackson angle).

(2) In the double resonance production region [$M(K^+\pi^-) < 1.54$ GeV], the $|t'|$ distribution is different for the forward and the backward $K\pi$ decay angular regions. Specifically, for the events with $\cos\theta < 0.5$ (a cut which tends to eliminate the $\Delta^{++}\pi^-$ enhancement), there is a clear break in the slope of the $|t'|$ distribution near 0.05 $(\text{GeV}/c)^2$. For events with $M(K^+\pi^-) \geq 1.54$ GeV the $|t'|$ distribution is relatively flat and fits the form $e^{at'}$ well.

(3) Events with $|t'| < 0.1$ $(\text{GeV}/c)^2$ and with $|t'| \geq 0.1$ $(\text{GeV}/c)^2$ show very different distributions in $K\pi$ mass, in $\cos\theta$, and in the correlation between $\cos\theta$ and φ, the Treiman-Yang angle.

These observations are studied and discussed in terms of contributions from resonance production by pion and other meson exchange diagrams and interference effects between these processes.

(4) There is a very rapid change in the $K\pi$ decay asymmetry in the region of the K^{*o}_{890}, and a similar change in the region of the K^{*o}_{1420}.

This experiment was carried out in the Brookhaven National Laboratory 80-inch hydrogen bubble chamber, which was exposed to a 9-GeV/c rf-separated K^+ beam at the AGS. The measurements were performed with the Lawrence Radiation Laboratory Flying-Spot Digitizer (FSD), and the geometric reconstruction and kinematical fitting were accomplished with the program SIOUX. The experimental details are given in ref. 5, which treated about half the present complete sample.

2. Data Analysis

2.1. The $K^+p \to K^+\pi^-\pi^+p$ Reaction

Figure 1 shows the triangle plot for $M(K^+\pi^-)$ versus $M(p\pi^+)$. We observe clear Δ^{++} and K^{*o}_{890} bands, which contain about 61% of the events in the $K^+\pi^-\pi^+p$ final state. These two bands are close to the kinematical boundary of the triangle plot. Inside the K^{*o}_{890} band, events with a high $M(p\pi^+)$ value are associated primarily with the Q enhancement, which has been discussed previously[5,6]. In this paper we study the events in the Δ^{++} band. In this band about 46% of the events are produced together with the K^{*o}_{890} and the K^{*o}_{1420} resonances. Figures 2a and 2b show the mass projections of the triangle plot. The Δ^{++}, K^{*o}_{890}, and K^{*o}_{1420} resonances are clearly observed.

2.2. $K^+\pi^-\Delta^{++}$ Dalitz Plot

Figure 3a shows the Dalitz plot for the $K^+\pi^-\Delta^{++}$ final state. From this plot we see that the effect of the $\Delta^{++}\pi^-$ low-mass enhancement extends down to the $K\pi$ threshold and contributes to at least part of the well-known positive asymmetry in $\cos\theta$ in the K^*_{890} and K^*_{1420} resonance regions[4]. Figure 3b shows the Dalitz plot with $|t'| < 0.1\ (\mathrm{GeV}/c)^2$. There is still a substantial population between the K^*_{890} and K^*_{1420} bands. Furthermore, although the $\Delta^{++}\pi^-$ low-mass enhancement is considerably reduced it is not eliminated by this cut.

To demonstrate the similarity between the $K^+\pi^-\Delta^{++}$ and $K^{*o}_{890}\,\pi^+p$ channels, we show the Dalitz plot for the latter in fig. 4. The K^{*o}_{890} is defined as $0.84 \leq M(K^+\pi^-) < 0.94$ GeV. There is a strong Δ^{++} band and a low-mass enhancement, the Q, in the $K^{*o}\pi^+$ system.

In order to determine the isospin of the $\Delta^{++}\pi^-$ enhancement, we compare the $\Delta^{++}\pi^-$ mass spectrum from both $K^o\pi^o\Delta^{++}$ and $K^+\pi^-\Delta^{++}$ final states as shown in fig. 5. We note that for the reactions $K^+p \to K^o\pi^o\Delta^{++}$ and

$K^+p \to K^+\pi^-\Delta^{++}$, the initial channel has a unique isospin state, namely $I = 1$, $I_z = 1$. Conservation of I and I_z requires $I = 3/2$ for the $\Delta^{++}\pi^o$ system and $I = 3/2$ or $1/2$ for the $\Delta^{++}\pi^-$ system. Since there is no excess of events near 1.58 GeV in the $M(\Delta^{++}\pi^o)$ plot (fig. 5a) and the Clebsch-Gordan coefficients for an $I = 3/2$ $(\Delta\pi)$ system predict a ratio of 9 to 2 for the intensity of the $\Delta^{++}\pi^o$ and $\Delta^{++}\pi^-$ states, the $\Delta^{++}\pi^-$ low-mass enhancement is predominantly $I = 1/2$. A simple double-Regge-pole exchange model, a diagram (shown in fig. 6a) with a Pomeranchuk exchange (P) at the K^+ vertex, pion exchange at the p vertex, and the π^- coupled to the P and pion trajectories at the interior vertex, can be shown to account for the dominant characteristics of this enhancement. The detailed discussion of the low-mass $\Delta^{++}\pi^-$ enhancement in terms of this double-Regge exchange diagram is given in a separate communication[7]).

Figure 6b shows a single exchange diagram for K^* resonance production. In addition to the pion there are four other allowed Regge trajectories, namely A_1, B, ρ, and A_2. At present there seems to be no clear understanding about the contributions of these allowed nonpion exchanges in this reaction. In the next section we outline a method for separating, at least in part, the pion and nonpion contributions. We emphasize the importance of achieving this separation cleanly in trying to fit the data to pion-exchange models.

2.3. $|t'|$ Distributions

Figure 7a shows the $|t'|$ distribution for the events with $M(K\pi) < 1.54$ GeV. The data are not consistent with one or even two exponential dependences. In order to investigate the production mechanism of the $K\pi$ system we study the structure of the $|t'|$ distribution as a function of $\cos\theta$. Figure 7b shows the $|t'|$ distribution for the events with $M(K^+\pi^-) < 1.54$ GeV and $\cos\theta < 0.5$. The straight lines represent the results of a least-squares fit to the data

for two functions of the form $e^{at'}$. We observe a very steep forward peak with slope $a = 23.6\pm5.2$ $(GeV/c)^{-2}$ for $|t'| < 0.05$ $(GeV/c)^2$, and a flatter distribution with slope $a = 9.5\pm2.0$ $(GeV/c)^{-2}$ for $|t'| \geq 0.05$ $(GeV/c)^2$. In contrast to this structure, the t' distribution for the events in the forward cos θ region (fig. 7c) appears quite different. The data in fig. 7c are fitted well by a single slope, $a = 13.5\pm1.2$ $(GeV/c)^{-2}$ for $|t'| < 0.3$ $(GeV/c)^2$. We shall associate this sharp forward peak with pion exchange. The lesser slope is due to the participation of nonpion exchanges (e.g., A_1, B, ρ, and A_2). Evidence for this assignment will be presented in the last paragraph of this section and in the next few sections.

Figure 7d shows the $|t'|$ distribution for the events with $M(K^+\pi^-) \geq 1.54$ GeV. The relative flatness of the slope, $a = 4.4\pm0.5$ $(GeV/c)^2$, can be qualitatively understood in two ways. One is that the high Kπ mass region is relatively far away from the pion pole. The other is due to the factor $(s/s_o)^{\alpha_\pi(t)}$ in the Regge amplitude. Here $\alpha_\pi(t)$ is the exchanged pion trajectory and t is the square of the four-momentum transfer from the target proton to the outgoing Δ^{++}. For the low Kπ mass region where a single exchange diagram (fig. 6b) dominates, s = (total energy)^2 is about $(4.25)^2$ $(GeV)^2$. For the high Kπ mass regions where the double exchange diagram (fig. 6a) dominates, $s = s_{\Delta^{++}\pi^-}$, which is about $(1.58)^2$ $(GeV)^2$. Therefore, due to the s-dependence factor the slope in the $|t|$ distribution for events with $M(K^+\pi^-) \geq 1.54$ GeV should be smaller than that for the events with $M(K^+\pi^-) < 1.54$ GeV by a factor $\approx 2\alpha'_\pi \ell n\,(4.25/1.58)^2 \approx 4$. Here we have used the linear form for the trajectory $\alpha_\pi = \alpha'_\pi(t - m_\pi^2)$, and have set $\alpha'_\pi = 1$ $(GeV/c)^{-2}$. The slopes in the $|t'|$ distributions should differ by a factor of the same order. Figure 7e is an enlargement of small $|t'|$ region of fig. 7b. The same phenomena are observed when we restrict the sample to events in the K^{*o}_{890} band, which represents about

33% of the events with $M(K^+\pi^-) < 1.54$ GeV. Figure 8a shows the $|t'|$ distribution for all the events in the K^*_{890} region.† In order to demonstrate that for K^*_{890} production there are other contributing mechanisms than pion exchange, we have also plotted the $|t'|$ distribution with $\cos\theta < -0.5$ for the K^{*o}_{890} band (fig. 8b). A break in slope near $|t'| = 0.05$ (GeV/c)^2 is observed here as well, in contrast to the straight-line $|t'|$ distribution in the other polar region ($\cos\theta \geq 0.5$) (fig. 8c). Figure 8d shows the $|t'|$ distribution for the events in the equatorial region $-0.5 \leq \cos\theta < 0.5$. The two slopes in fig. 8b are $a = 31.2\pm12.4$ (GeV/c)$^{-2}$ and $a = 7.1\pm3.1$ (GeV/c)$^{-2}$. The slope in fig. 8c is $a = 14.4\pm1.8$ (GeV/c)$^{-2}$. The values of these slopes are about the same as those for the events in the angular regions $\cos\theta < 0.5$ and $\cos\theta \geq 0.5$ with $M(K^+\pi^-) < 1.54$ GeV. This supports the assumption that the production mechanisms for the events with $M(K^+\pi^-) < 1.54$ GeV/c are the same as those for the events in the $K^{*o}_{890}\Delta^{++}$ double resonance region. For pure single resonance production the $|t'|$ distributions for two symmetrical polar regions should be the same if there are only single exchange diagrams contributing, such as those shown in fig. 6b. The different structures of $|t'|$ distributions in figs. 8b and 8c indicate that, even in the K^{*o}_{890} resonance region, there are nonnegligible contributions from other processes, e.g., the double peripheral exchange process shown in fig. 6a, or perhaps a $K\pi$ s wave. The change of the slope in fig. 8b is due to nonpion exchange. More evidence and discussion of these points is given in the study of $K\pi$ decay distributions in Sect. 2.4.

---

†For comparing data at different laboratory momenta, an effective four-momentum squared, $t_{eff} = t' + t'_m$, is the appropriate variable to use[8]). Here t'_m is defined as the mean value of t_m in the mass region considered. For $K^{*o}_{890}\Delta^{++}$, $t'_m \approx -0.024$ (GeV/c)^2 and for $K^{*o}_{1420}\Delta^{++}$, $t'_m \approx -0.044$ (GeV/c)^2.

2.4. Kπ Decay Angular Distributions

In this section we study the Kπ decay angular distributions in the K^* resonance region by fitting the distributions to a Legendre polynomial in cos θ to determine the various angular momentum components of the scattering amplitude. In addition, as an alternative procedure we assume a unique spin for the events in a K^* resonance region and study the decay distribution $W(\cos\theta,\varphi)$ in terms of the spin density matrix elements.

Figures 9a and 9b show the cos θ vs $M(K^+\pi^-)$ scatter plots for $|t'| < 0.1$ $(GeV/c)^2$ and $|t'| \geq 0.1$ $(GeV/c)^2$ respectively. The projections of the cos θ distributions in the K^{*o}_{890} and K^{*o}_{1420} bands with the same t' cuts are shown in Fig. 10a-d. We observe that the difference between the cos θ distributions in the K^*_{890} band with different $|t'|$ cuts is striking. For $|t'| < 0.1$ $(GeV/c)^2$, it is very much like $\cos^2\theta$, whereas for $|t'| \geq 0.1$ $(GeV/c)^2$, it is consistent with being flat. The curves in fig. 10a and c are the results of a least-squares fit to a sum of Legendre polynomials, $\sum_{\ell=0}^{n} a_\ell P_\ell(\cos\theta)$. The coefficients of the polynomial fits in the K^{*o}_{890} and K^{*o}_{1420} regions are given in table 1. From the values of these coefficients we obtain the well-known spin-parity assignment of $J^P = 1^-$ for K^*_{890}, and find that the result agrees with the assignment of $J^P = 2^+$ for K^*_{1420}.

Figure 11 shows the results from the fits of the second-order polynomial in cos θ for K^{*o}_{890} to our data excluding the very forward polar region (cos $\theta \geq 0.5$). As mentioned earlier, this cut eliminates most of the contribution from the double peripheral processes. The fit is normalized to the number of events in each $|t'|$ interval. If we assume pure pseudoscalar exchange, then a_2 and a_o indicate the contributions from Kπ p- and s-wave intensities respectively, and a_1 the interference between the p and s waves. However, we point out that if in addition there is a vector exchange, then its $\sin^2\theta$-decay distribution

added to the $\cos^2\theta$-decay distribution from the pseudoscalar exchange can fake an a_o term. We observe that a_o drops more slowly than a_1 or a_2. For $|t'| \geq 0.15$ $(GeV/c)^2$, (a_o/a_2) and (a_o/a_1) gradually increase, and presumably the nonpion exchanges become more important in this region. This indicates that in analyzing $K\pi$ scattering data the sample must be restricted to very small $|t'|$ values--at this momentum less than ≈ 0.05 $(GeV/c)^2$.

As a result of a fit to the decay angular distribution, we find $\rho_{oo} = 0.79\pm0.03$ for $|t'| < 0.1$ $(GeV/c)^2$ and $\rho_{oo} = 0.49\pm0.05$ for $|t'| \geq 0.1$ $(GeV/c)^2$. This is in agreement with our assignment of pion exchange for the sharp forward t' distribution in Fig. 7b. We emphasize that the presence of a distinct K^{*o}_{890} band in both t' regions indicates the dominance of K^{*o}_{890} over background (fig. 9a,b).

Figure 12 shows the spin density matrix elements ρ_{oo}, $\rho_{1,-1}$ and Re ρ_{10}, and fig. 13 shows $\sigma^{\pm} \equiv \frac{1}{2}(\rho_{1,1} \pm \rho_{1,-1})$ for the K^{*o}_{890} as a function of t', the values of which are given in table 2. The values of ρ_{oo} in fig. 12a indicate the unnatural parity contribution in the t channel; σ^+ and σ^- in fig. 13 indicate the natural and unnatural parity contributions in the t-channel helicity state ± 1. In this reaction the unnatural parity exchanges are the π and A_1 and the natural parity exchanges are the ρ and A_2. With our statistical uncertainties and the background problem we can only make some qualitative statements:

(a) ρ_{oo} is large in the forward direction and decreases to a small value as $|t'|$ increases. This again indicates that the K^{*o}_{890} is produced in the $m = 0$ state in the forward direction for which only pion exchange contributes.

(b) Both the natural-parity and the unnatural-parity exchanges contribute to K^{*o}_{890} production in the $m = \pm 1$ states. The contributions are of the same order and increase as $|t'|$ increases. With the present data it is difficult to determine the cause or validity of the apparent nonzero values for $\sigma^{\pm}$ in the forward direction.

(c) Re $\rho_{1,0}$ is always negative and not negligible.

Figure 14 shows the cos θ-φ decay angular correlation plots for events in the two K^* resonance regions with $|t'| < 0.1$ (GeV/c)^2 and $|t'| \geq 0.1$ (GeV/c)^2. The sharp change in the character of the correlation with t' for each resonance indicates either the presence of at least two production mechanisms for each resonance, or the interference of the dominant wave in each resonance (1^- for K^*_{890} and 2^+ for K^*_{1420}) with a background term of opposite parity and with a markedly different t' dependence from the resonance itself. This may also be seen in the nonzero values for $\rho_{1,-1}$ and Re ρ_{10} shown in table 2. Figure 15 shows the decay angular distributions, cos θ, for the Δ^{++} in the final state $K^{*o}_{890}\Delta^{++}$ for $|t'| < 0.1$ (GeV/c)^2 and $|t'| \geq 0.1$ (GeV/c)^2. The striking difference in distributions is additional evidence for the presence of different production mechanisms dominating the high $|t'|$ and low $|t'|$ regions.[†]

[†]The curves shown in fig. 15 are results of the least-square fits to the decay angular distributions with spin density matrix elements $\rho_{33} = 0.05\pm0.03$, $\rho_{11} = 0.45\pm0.03$, Re $\rho_{3,-1} = -0.08\pm0.03$, and Re $\rho_{3,1} = -0.06\pm0.03$ for $|t'| < 0.1$ (GeV/c)^2, and $\rho_{33} = 0.17\pm0.03$, $\rho_{11} = 0.33\pm0.03$, Re $\rho_{3,-1} = -0.07\pm0.04$, and Re $\rho_{3,1} = -0.08\pm0.04$ for $|t'| \geq 0.1$ (GeV/c)^2.

2.5. The Asymmetry and the Mass Spectrum of the Kπ System

2.5.1. Kπ Asymmetry

Figure 16 shows a forward-backward asymmetry plot for the Kπ system as a function of Kπ mass. The asymmetry is defined as (F-B)/(F+B), where F and B refer to the forward and backward events in θ. We observe that just above the K^*_{890} the asymmetry goes to zero very rapidly from a positive value, and then increases rather smoothly to positive values again for higher Kπ masses

except for a small perturbation on passing the K^*_{1420}. The large positive asymmetry for $M(K^+\pi^-) \geq 1.54$ GeV indicates that the K^+ goes forward and the π^- backward in the $K\pi$ rest frame. Here the backward π^- is associated with the low-mass $\Delta^{++}\pi^-$ enhancement. The rapid change in asymmetry just above the K^*_{890} can be attributed to the interference of the K^*_{890} with (i) some $K\pi$ partial waves of parity opposite to that of the K^*_{890} ($J^P = 1^-$) or (ii) the process which leads to the $\Delta^{++}\pi^-$ mass enhancement as shown in Sect. 2.2, or both. Trippe et al., in an analysis of the same four-body reaction at 7.3 GeV/c, deduced an s-wave $K\pi$ resonance at a mass of ≈ 1.1 GeV and with a width of ≈ 0.4 GeV on the basis of an application of the Duerr-Pilkuhn method to an OPE model[1]). Also Antich et al. have claimed[2]) the existence of a $J^P = 1^-$ wave in the neighborhood of the K^*_{1420} which interferes with the dominant $J^P = 2^+$ wave to give the observed asymmetry in this region. In addition, several K-nucleon experiments leading to three particles in the final state have shown indications of the $K\pi$ mass peaks in this region. These indications were for narrow ($\Gamma \approx 0.1$ GeV) peaks at $M(K^+\pi^-) = 1.26\pm0.02$ GeV in the reaction $K^+p \to K^o\pi^+p$ at 3.9 GeV/c[3a]), at $M(K^+\pi^-) = 1.16\pm0.01$ GeV in the reaction $K^-n \to K^o\pi^-n$ at 3.9 GeV/c[3b]), and at ≈ 1.08 GeV in $K^+p \to K^o\pi^+p$ at 3.5 GeV/c and 3.9 GeV/c[3a,c]).

We have also studied the asymmetry as a function of t', and within the limited statistics we observe: (a) at small $|t'|$ values the variation in asymmetry at the K^*_{1420} resembles that at the K^*_{890}, and (b) at large $|t'|$ values both these rapid variations in asymmetry are reduced.

2.5.2. Kπ Mass Spectrum

Figure 17a shows the $K^+\pi^-$ mass distribution for all our events; fig. 17b for $|t'| < 0.1$ (GeV/c)^2, and fig. 17c for $|t'| \geq 0.1$ (GeV/c)^2. The shaded

histograms have the cut $\cos\theta < 0.5$, in order to reduce the contribution from the low-mass $\Delta^{++}\pi^-$ enhancement. We make the following observations: (a) In both the unshaded and the shaded histograms in fig. 17b [$|t'| < 0.1$ (GeV/c)^2] the background between the two well-known K^*'s is very large in comparison with that part of the mass spectrum above the K^*_{1420}. Since an s-wave $K\pi$ system can couple only to pion exchange and the region $|t'| < 0.1$ (GeV/c)^2 is dominated by pion exchange, it may be reasonable to associate at least part of this plateau with an s-wave $K\pi$ system. Whether the various mass peaks reported in the $K\pi N$ channel[3]) have any relevance to this high plateau is unclear at present. (b) In the unshaded histogram in fig. 17c [$|t'| \geq 0.1$ (GeV/c)^2] the background between the two K^*'s appears to join smoothly with the mass spectrum in the high $K\pi$ mass region. In addition, a small mass peak is seen at a mass of about 1.1 GeV, where a change in the decay angular distribution is also observed, as mentioned in the preceding section. This mass peak at 1.1 GeV shows more prominently in the shaded histogram in fig. 17c, where the effects of the low-mass $\Delta^{++}\pi^-$ enhancement have been reduced. This could be the same enhancement as those in the 1080—1160-MeV region mentioned in Ref. 3a,c, but present statistics do not permit a definitive statement. Since this enhancement appears only for $|t'| \geq 0.1$ (GeV/c)^2, it is presumably produced by a non-pion-exchange mechanism. The shaded histogram in fig. 17c shows a greater number of events in the plateau than in the region above the K^*_{1420}, but the effect is somewhat reduced here. Since the plateau in Fig. 17c, where pion exchange is very suppressed, cannot be due to s wave, and there is an indication of a narrow mass peak at 1.1 GeV here, possible higher spin resonances in this region may be the explanation. (c) All the discussions above agree with the assignment of the forward t' peak as due to pion exchange, and the region with lesser slope as due to the participation of nonpion exchanges. We note that Trippe et al.[1])

in their OPE analysis of this Kπ mass region have used data with $|t|$ as large as 0.5 $(GeV/c)^2$, which, on the basis of the present work, must contain considerable contributions from non-pion-exchange mechanisms that cannot lead to s-wave Kπ scattering.

3. Conclusions

We conclude:

1. Pion exchange appears to dominate the reaction $K^+p \to K^+\pi^-\Delta^{++}$ for $|t'| < 0.1$ $(GeV/c)^2$, but nonpion exchanges become important for $|t'| \geq 0.1$ $(GeV/c)^2$. This has been demonstrated in studies of the t' distributions, the decay angular distributions of the Kπ system, and the spin-density matrix elements.

2. The well-known asymmetry in the Kπ decay angular distribution is due to the interference of the dominant resonant waves for the K^*_{890} and K^*_{1420} with background terms. We note that the observed asymmetries in the K^*_{890} and K^*_{1420} region require an even-parity background term under the K^*_{890} (s wave?) and an odd-parity background term under the K^*_{1420} (p wave?). Although we cannot ascertain whether these background terms are due to (i) two new resonances, or (ii) the low-mass $\Delta^{++}\pi^-$ enhancement, or both, we emphasize the importance of accounting for the various origins of this asymmetry in any analysis of Kπ scattering.

3. The plateau in the Kπ mass spectrum between the K^*_{890} and K^*_{1420} is associated primarily with the low $|t'|$ region and thus could be due in part to s wave. There may also be contributions from the possible resonances reported in Ref. 3. In our work there is some evidence for an enhancement at 1.1 GeV in the data with $|t'| \geq 0.1$ $(GeV/c)^2$, but the statistics are not conclusive.

We thank R. Shutt and the staff of the 80-inch bubble chamber and H. Foelsche and the AGS staff at Brookhaven for helping with the exposure. We acknowledge the valuable support given by H. White and the FSD staff and by our programming and scanning staff, in particular Emmett R. Burns.

References

1) T. G. Trippe, C.-Y. Chien, E. Malamud, J. Mellema, P. E. Schlein, W. E. Slater, D. H. Stork and H. K. Ticho, Phys. Letters 28B (1968) 203.

2) P. Antich, A. Callahan, R. Carson, B. Cox, D. Denegri, L. Ettlinger, D. Gillespie, G. Goodman, G. Luste, R. Mercer, A. Pevsner and R. Zdanis, Phys. Rev. Letters 21 (1968) 842.

3) a) W. P. Dodd, T. Joldersma, R. B. Palmer and N. P. Samios, Phys. Rev. 177 (1969) 1991;

b) David J. Crennell, Uri Karshon, Kwan Wu Lai, John S. O'Neall and J. Michael Scarr, Phys. Rev. Letters 22 (1969) 487;

c) W. de Baere, J. Debaisieux, P. Dufour, F. Grard, J. Heughebaert, L. Pape, P. Peeters, F. Verbeure, R. Windmolders, Y. Goldschmidt-Clermont, V. P. Henri, B. Jongejans, A. Moiseev, F. Muller, J. M. Perreau, A. Prokes, and V. Yarba, Nuovo Cimento 51A (1967) 401.

4) C. Fu, A. Firestone, G. Goldhaber, G. H. Trilling and B. C. Shen, Contribution to the Informal Meeting on Experimental Meson Spectroscopy, Philadelphia, April 1968 (UCRL-18201, April 1968).

5) G. Goldhaber, A. Firestone, and B. C. Shen, Phys. Rev. Letters 19 (1967) 972.

6) G. Alexander, A. Firestone, G. Goldhaber, and D. Lissauer, Nuclear Physics B13 (1969) 503.

7) C. Fu and E. Berger, Double peripheral model analysis of $K^+p \rightarrow K^+\pi^-\Delta^{++}_{1236}$ at 9 GeV/c (in preparation).

8) G. Goldhaber, W. R. Butler, D. G. Coyne, B. H. Hall, J. N. MacNaughton and G. H. Trilling, Phys. Rev. Letters (in press).

Table 1. Coefficients of $\sum_{\ell=0} a_\ell P_\ell(\cos\theta)$ for the K^*'s with $|t'| < 0.1$ (GeV/c)^2.

(a) K^*_{890}

a_0	a_1	a_2	a_3	a_4
1.0	0.73±0.06	1.33±0.06		
1.0	0.70±0.07	1.31±0.06	-0.09±0.09	
1.0	0.69±0.07	1.34±0.08	-0.08±0.10	0.06±0.11

(b) K^*_{1420}

a_0	a_1	a_2	a_3	a_4	a_5	a_6
1.0	0.63±0.09	1.90±0.09	0.20±0.11	1.23±0.13		
1.0	0.68±0.10	2.06±0.08	0.18±0.14	1.35±0.12	0.41±0.13	
1.0	0.67±0.10	2.14±0.10	0.21±0.16	1.68±0.16	0.20±0.14	0.59±0.15

Table 2. Spin density matrix elements and $\sigma^{\pm}$ for K^{*o}_{890}.

$\lvert t' \rvert$	$\rho_{m,m'}$					
	$\rho_{0,0}$	Re $\rho_{1,0}$	$\rho_{1,-1}$	$\rho_{1,1}$	σ^{+}	σ^{-}
0.00-0.04	0.80±0.04	-0.02±0.03	0.03±0.03	0.10±0.04	0.06±0.02	0.04±0.02
0.04-0.10	0.76±0.05	-0.15±0.03	-0.05±0.03	0.12±0.05	0.03±0.02	0.09±0.02
0.10-0.20	0.67±0.05	-0.23±0.03	-0.08±0.04	0.17±0.05	0.04±0.02	0.13±0.03
0.20-0.35	0.39±0.09	-0.15±0.05	0.02±0.08	0.31±0.09	0.16±0.04	0.14±0.04
0.35-0.60	0.30±0.10	-0.20±0.04	0.05±0.09	0.35±0.10	0.20±0.05	0.15±0.05

Figure Captions

Fig. 1. Triangle plot for $M(K^+\pi^-)$ vs $M(p\pi^+)$.

Fig. 2. (a) The $K^+\pi^-$ mass projection of Fig. 1. (b) The $p\pi^+$ mass projection of Fig. 1.

Fig. 3. Dalitz plots for the $K^+\pi^-\Delta^{++}$ final state with (a) no $|t'|$ cut and (b) a cut, $|t'| < 0.1$ $(GeV/c)^2$.

Fig. 4. The Dalitz plot for the K^{*o}_{890} π^+p final state.

Fig. 5. (a) The $\Delta^{++}\pi^o$ mass spectrum for the final state $K^o\pi^o\Delta^{++}$. (b) The $\Delta^{++}\pi^-$ mass spectrum for the final state $K^+\pi^-\Delta^{++}$.

Fig. 6. (a) A double-Regge-pole-exchange diagram associated with the low $\Delta^{++}\pi^-$ mass enhancement (for the $K^+\pi^-\Delta^{++}$ channel). (b) A single exchange diagram for K^* resonance productions (for the $K^+\pi^-\Delta^{++}$ channel).

Fig. 7. (a) The $|t'|$ distribution for the events with $M(K^+\pi^-) < 1.54$ GeV. (b) The $|t'|$ distribution for the events with $M(K^+\pi^-) < 1.54$ GeV and $\cos\theta < 0.5$. (c) The $|t'|$ distribution for the events with $M(K^+\pi^-) < 1.54$ GeV and $\cos\theta \geq 0.5$. (d) The $|t'|$ distribution for the events with $M(K^+\pi^-) > 1.54$ GeV and $\cos\theta \geq 0.5$. Actually most of the events with $M(K^+\pi^-) > 1.54$ GeV are in the forward $\cos\theta$ region. (e) The same $|t'|$ distribution as Fig. 7a with a large scale. For showing the change of the slope only the forward region [$|t'| < 0.2$ $(GeV/c)^2$] is plotted.

Fig. 8. (a) $|t'|$ distribution for all the events in the K^*_{890} region, (b) $\cos\theta < -0.5$, (c) $\cos\theta \geq 0.5$, and (d) $-0.5 \leq \cos\theta < 0.5$.

Fig. 9. $\cos\theta$ vs $M(K^+\pi^-)$ scatter plots for events with (a) $|t'| < 0.1$ $(GeV/c)^2$ and (b) $t' \geq 0.1$ $(GeV/c)^2$.

Fig. 10. $\cos\theta$ distributions for the events in the K^*_{890} region with (a) $|t'| < 0.1$ $(GeV/c)^2$ and (b) $|t'| \geq 0.1$ $(GeV/c)^2$ and $\cos\theta$ distributions for the events in the K^*_{1420} (1.34-1.50 GeV) region with (c) $|t'| < 0.1$ $(GeV/c)^2$ and (d) $|t'| \geq 0.1$ $(GeV/c)^2$.

Fig. 11. The coefficients of the expansion $\Sigma a_n \cos^n \theta$ for the events in the K^*_{890} region with $\cos\theta < 0.5$. (a) a_o, (b) a_1 and (c) b_2.

Fig. 12. Spin density matrix elements (a) ρ_{00}, (b) $\rho_{1,-1}$ and (c) Re ρ_{10} for K^{*o}_{890} as functions of t'.

Fig. 13. (a) σ^+ and (b) σ^- for K^{*o}_{890} as functions of t'.

Fig. 14. $\cos\theta$-φ decay angular correlation plots for the events in the K^{*o}_{890} region with (a) $|t'| < 0.1$ $(GeV/c)^2$ and (b) $|t'| \geq 0.1$ $(GeV/c)^2$ and $\cos\theta$-φ decay angular correlation plots for the events in the K^{*o}_{1420} region with (c) $|t'| < 0.1$ $(GeV/c)^2$ and (d) $|t'| \geq 0.1$ $(GeV/c)^2$.

Fig. 15. The decay angular distribution, $\cos\theta(p\pi^+)$, for the Δ^{++} resonance with (a) $|t'| < 0.1$ $(GeV/c)^2$ and (b) $|t'| \geq 0.1$ $(GeV/c)^2$. Here $\cos\theta(p\pi^+)$ is the Jackson angle for the $p\pi^+$ system.

Fig. 16. The forward-backward asymmetry $(\frac{F-B}{F+B})$ plot for the $K^+\pi^-$ system as a function of $K^+\pi^-$ mass.

Fig. 17. The $K^+\pi^-$ mass distributions with the cuts (a) no t' cut, (b) $|t'| < 0.1$ $(GeV/c)^2$ and (c) $|t'| \geq 0.1$ $(GeV/c)^2$. The shaded portion of the histograms correspond to the events in the region with $\cos\theta < 0.5$.

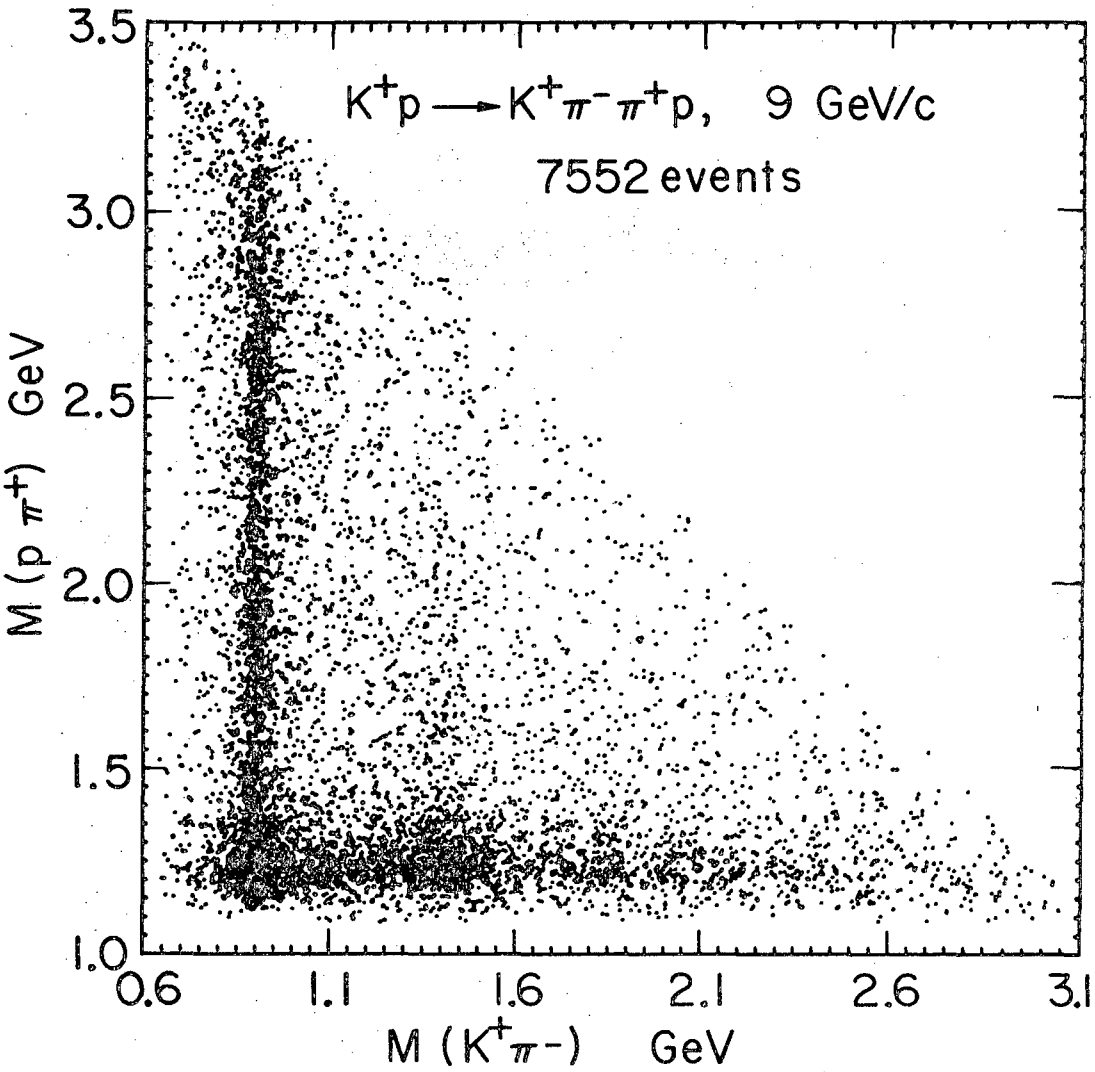

XBL696-3049

Fig. 1

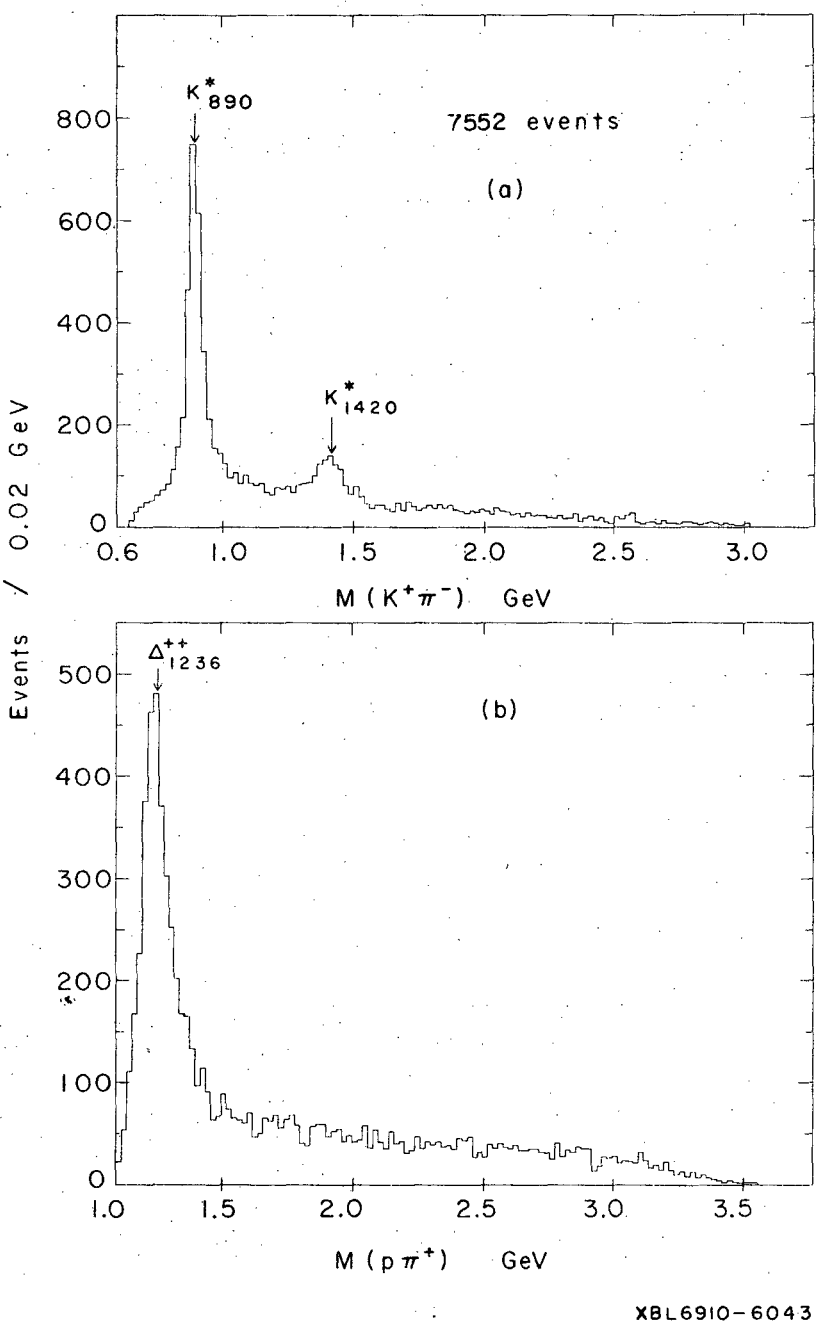
K*890
7552 events
(a)
K*1420
800
600
400
200
0
0.6
1.0
1.5
2.0
2.5
3.0
Events / 0.02 GeV
M (K+π−) GeV
Δ++1236
(b)
500
400
300
200
100
0
1.0
1.5
2.0
2.5
3.0
3.5
M (pπ+) GeV
XBL6910-6043

Fig. 2

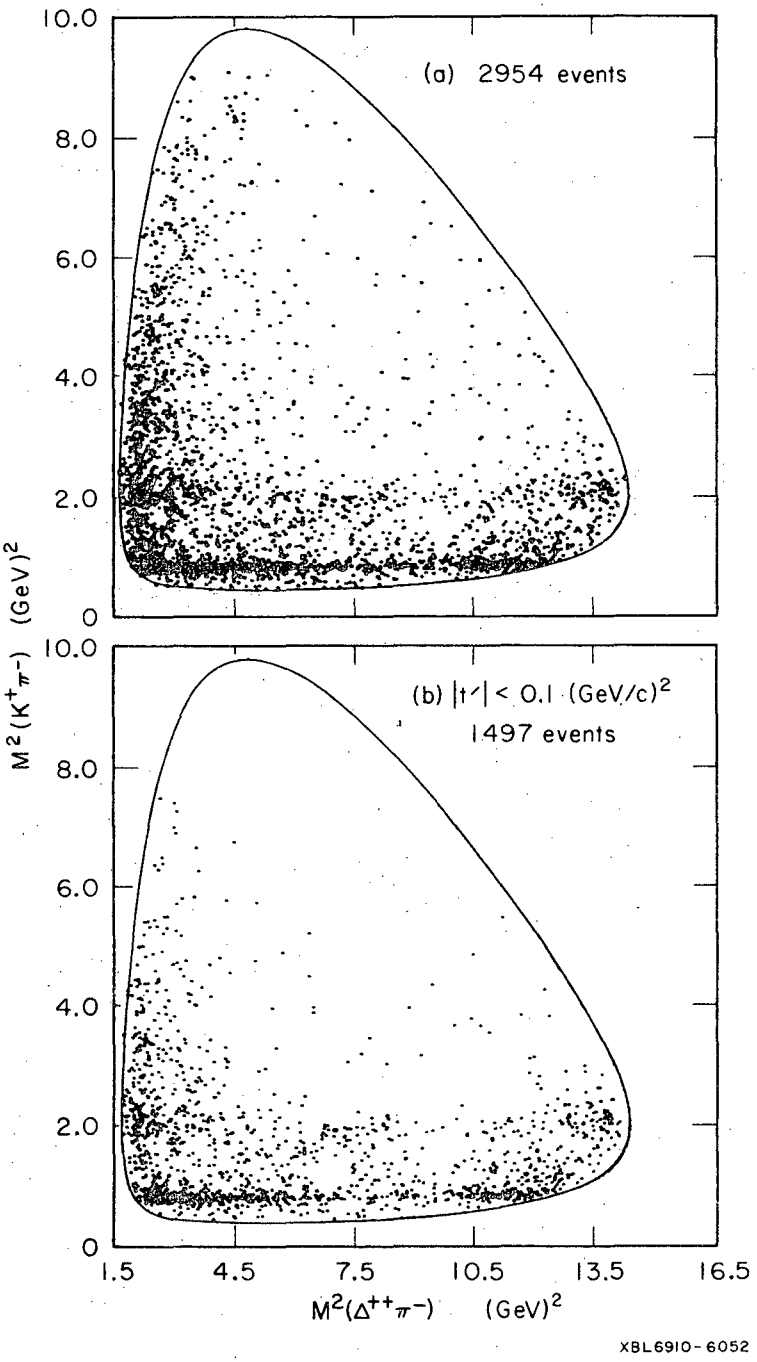
(a) 2954 events
(b) |t'| < 0.1 (GeV/c)²
1497 events
M²(K⁺π⁻) (GeV)²
M²(Δ⁺⁺π⁻) (GeV)²
10.0
8.0
6.0
4.0
2.0
0
1.5
4.5
7.5
10.5
13.5
16.5
XBL6910-6052

Fig. 3

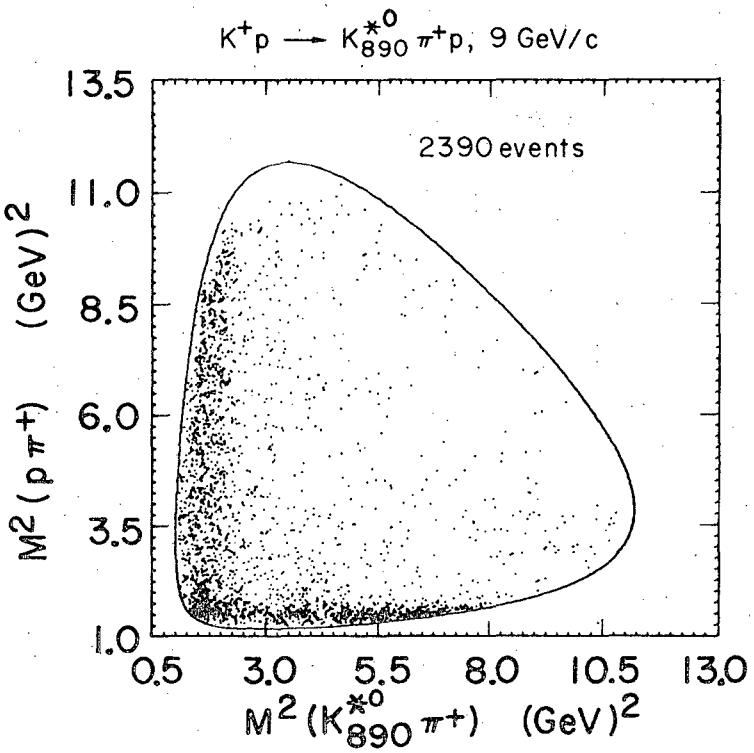

XBL 6911-6310

Fig. 4

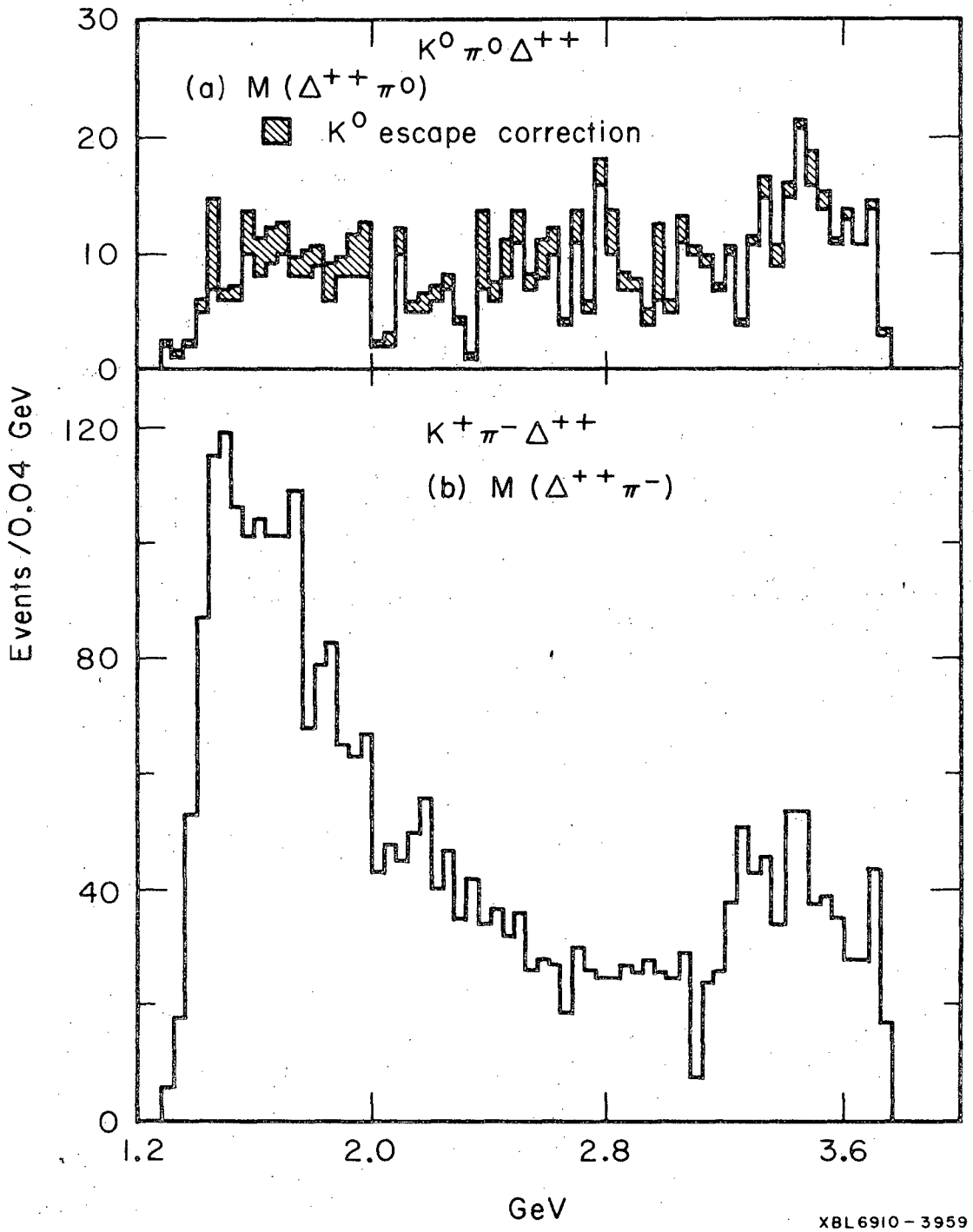
$K^0 \pi^0 \Delta^{++}$
(a) M ($\Delta^{++} \pi^0$)
K^0 escape correction
$K^+ \pi^- \Delta^{++}$
(b) M ($\Delta^{++} \pi^-$)
Events /0.04 GeV
GeV
1.2
2.0
2.8
3.6
0
10
20
30
40
80
120
XBL6910-3959

Fig. 5

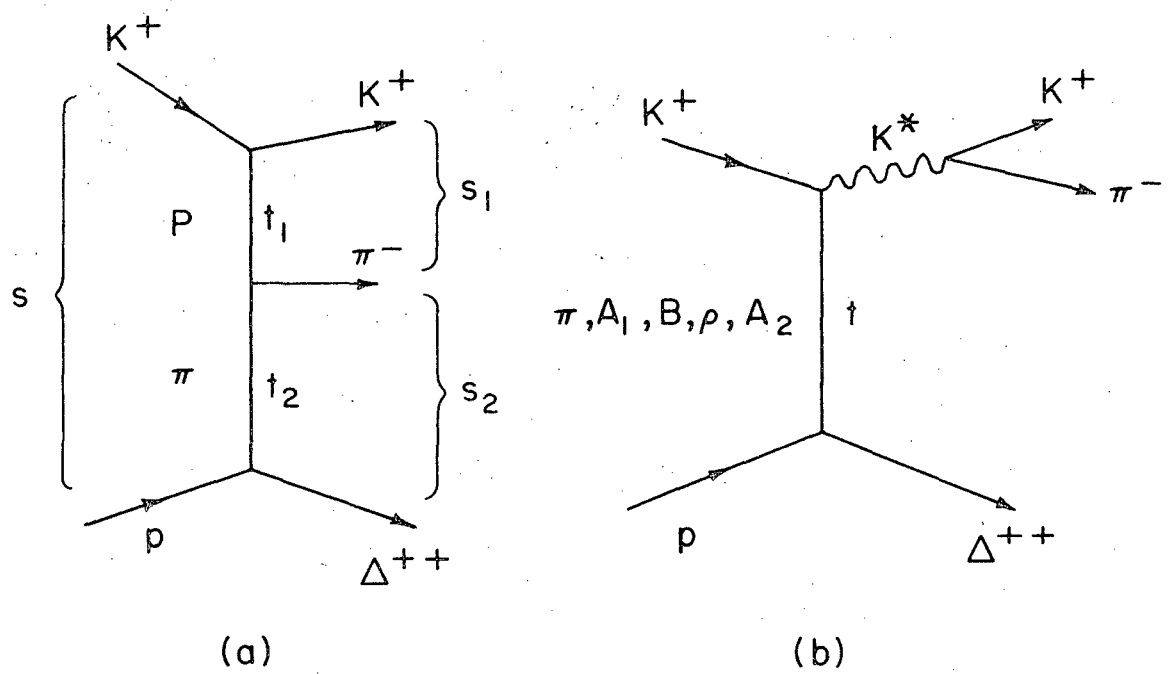

XBL 6910-3958

Fig. 6

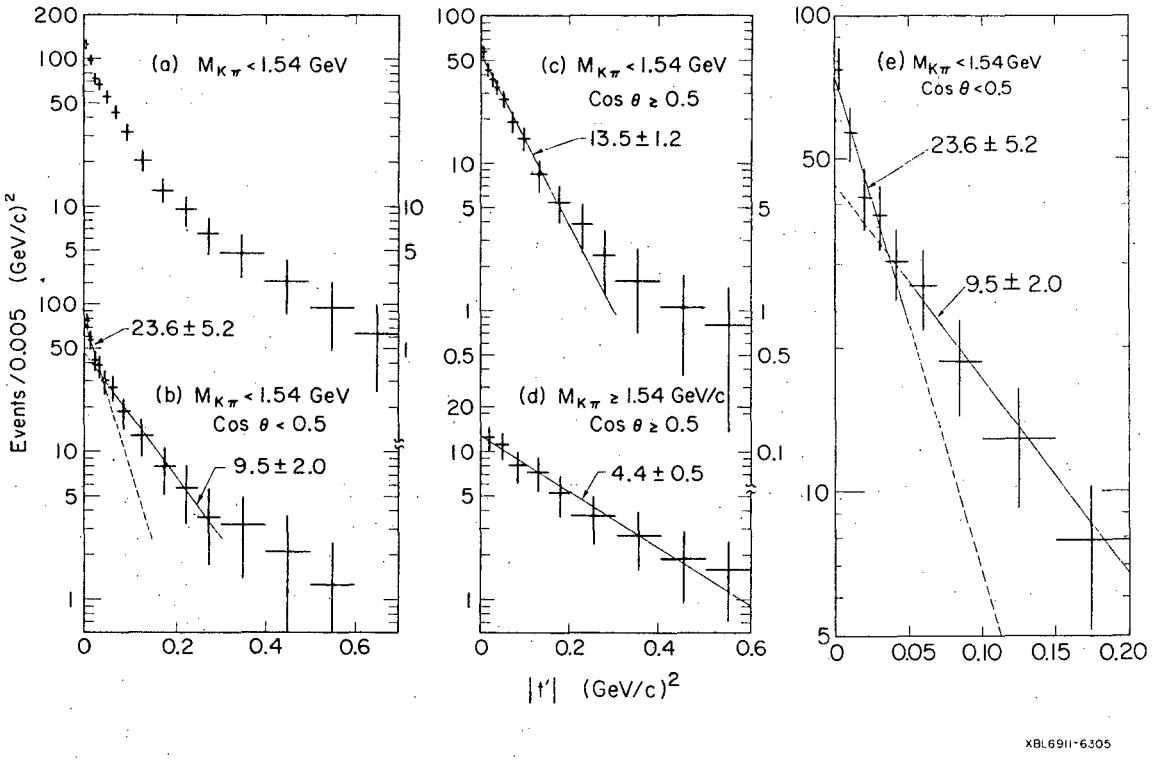
(a) $M_{K\pi} < 1.54$ GeV
23.6 ± 5.2
(b) $M_{K\pi} < 1.54$ GeV
Cos θ < 0.5
9.5 ± 2.0
(c) $M_{K\pi} < 1.54$ GeV
Cos θ ≥ 0.5
13.5 ± 1.2
(d) $M_{K\pi} \geq 1.54$ GeV/c
Cos θ ≥ 0.5
4.4 ± 0.5
(e) $M_{K\pi} < 1.54$ GeV
Cos θ < 0.5
23.6 ± 5.2
9.5 ± 2.0
Events / 0.005 (GeV/c)²
|t'| (GeV/c)²
XBL6911-6305

Fig. 7

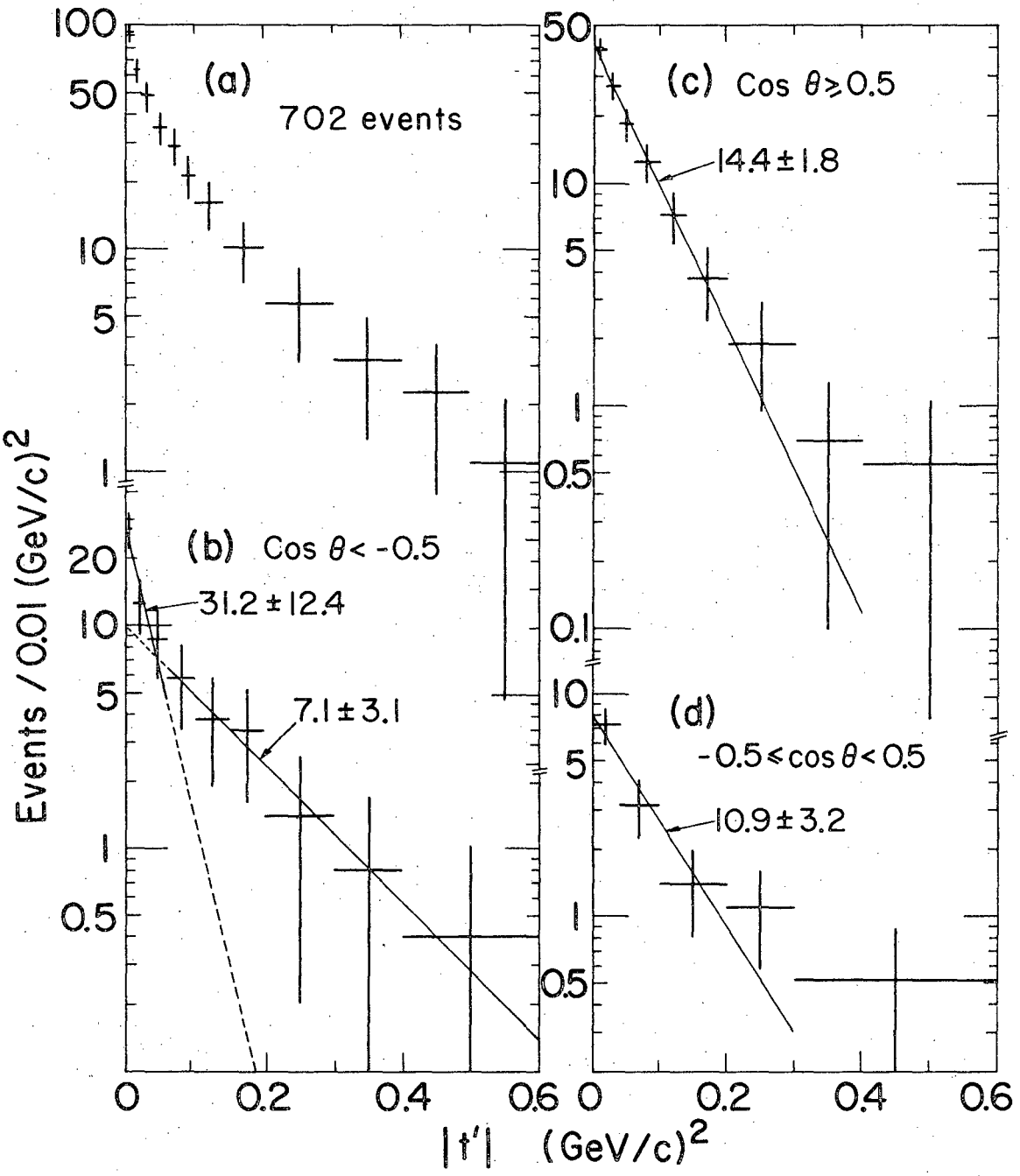
(a)
702 events
(b) Cos θ< -0.5
31.2 ± 12.4
7.1 ± 3.1
(c) Cos θ≥0.5
14.4 ± 1.8
(d)
-0.5≤cos θ< 0.5
10.9 ± 3.2
Events / 0.01 (GeV/c)²
|t'| (GeV/c)²
XBL6911-6306

Fig. 8

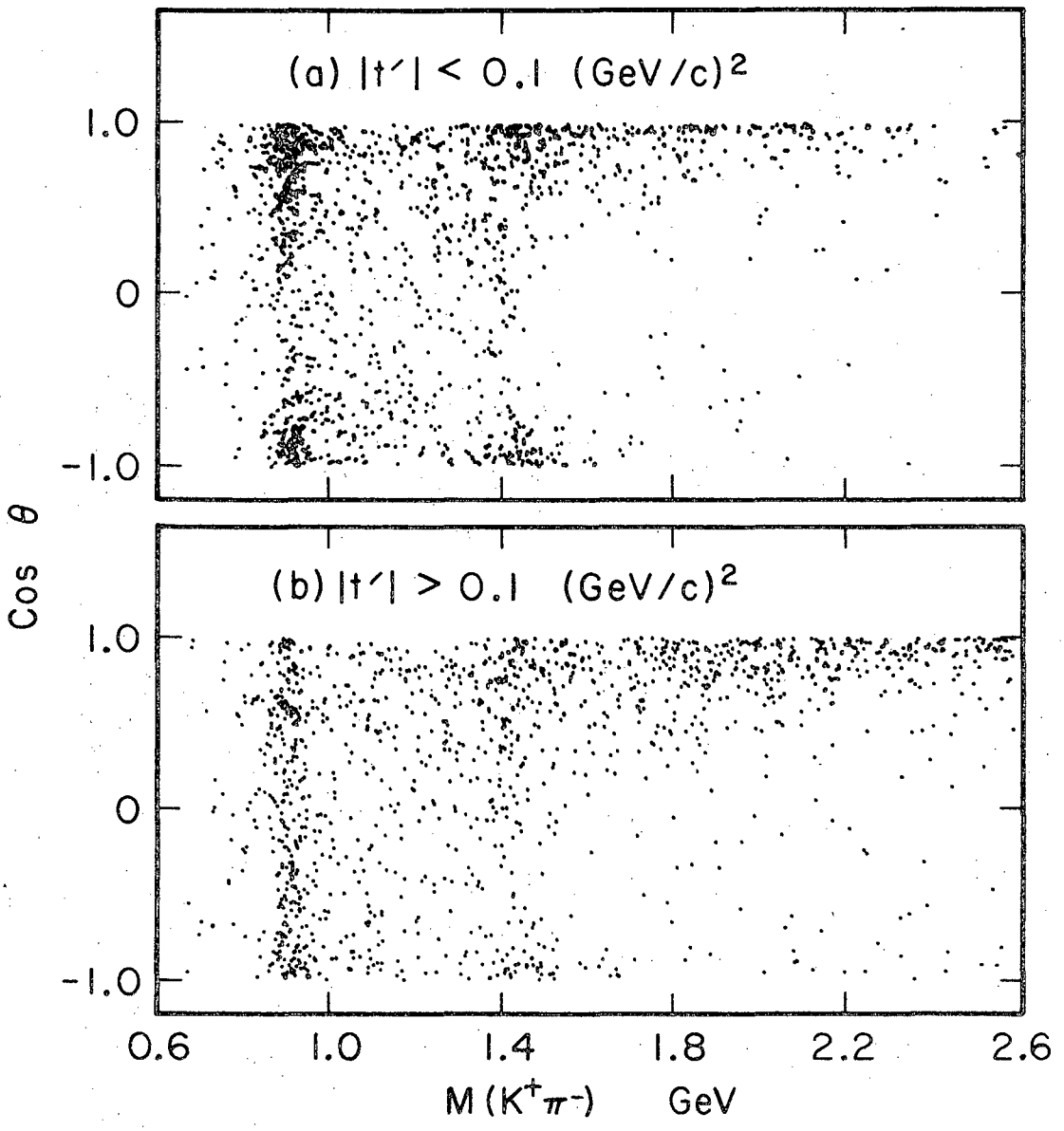
(a) |t′| < 0.1 (GeV/c)²
(b) |t′| > 0.1 (GeV/c)²
Cos θ
1.0
0
-1.0
0.6
1.0
1.4
1.8
2.2
2.6
M(K⁺π⁻) GeV
XBL6910-6053

Fig. 9

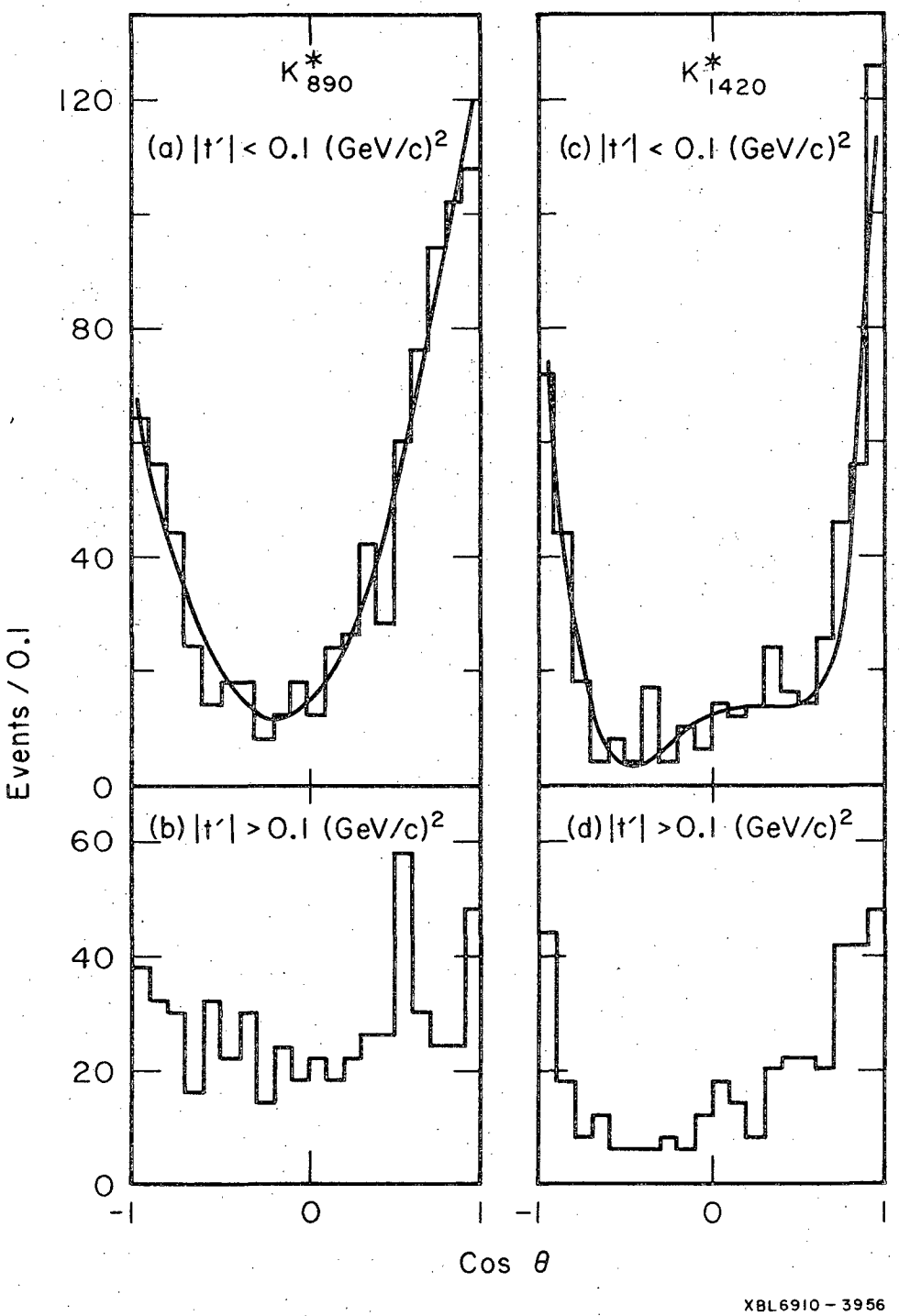
K*890
K*1420
(a) |t'| < 0.1 (GeV/c)²
(c) |t'| < 0.1 (GeV/c)²
(b) |t'| > 0.1 (GeV/c)²
(d) |t'| > 0.1 (GeV/c)²
Events / 0.1
Cos θ
XBL6910-3956

Fig. 10

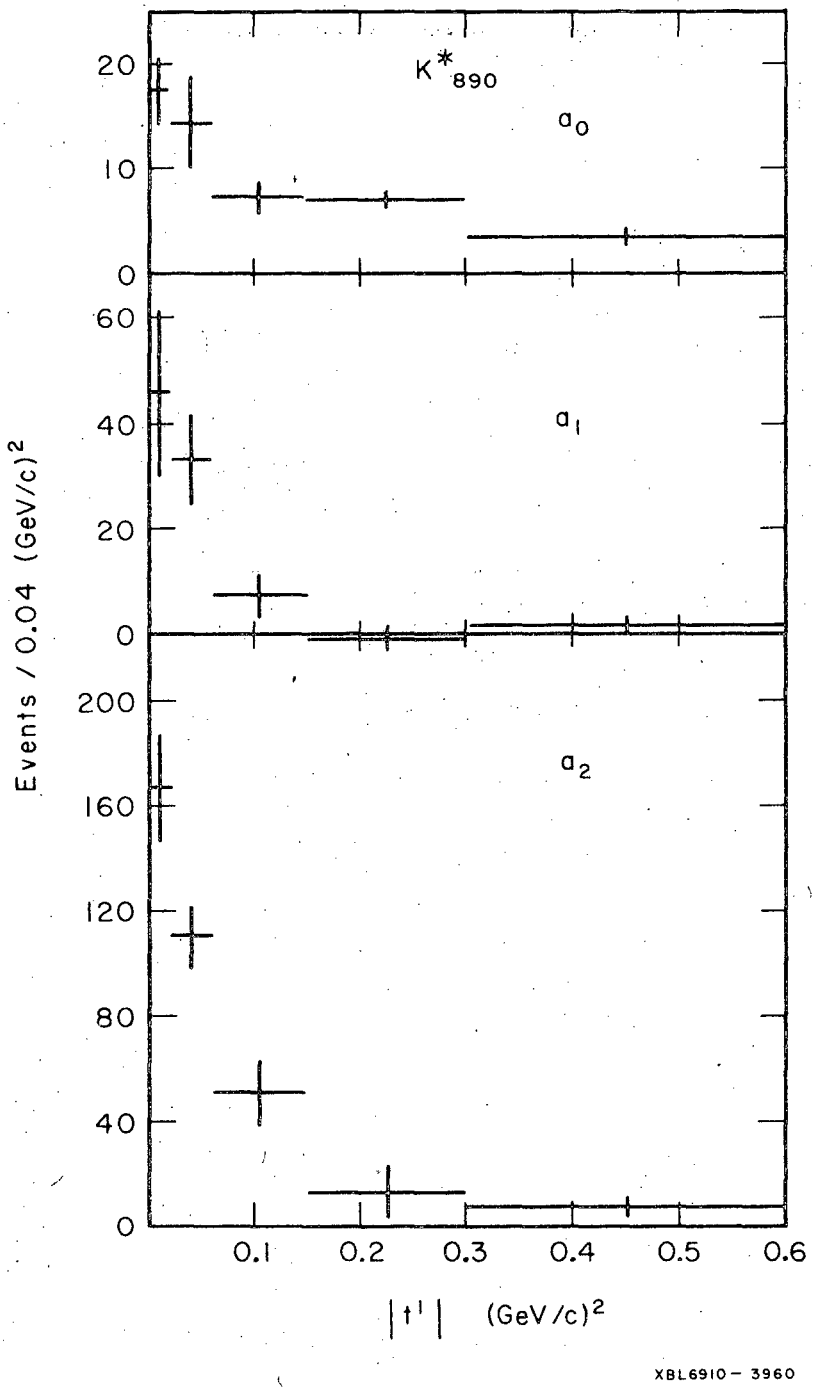

Fig. 11

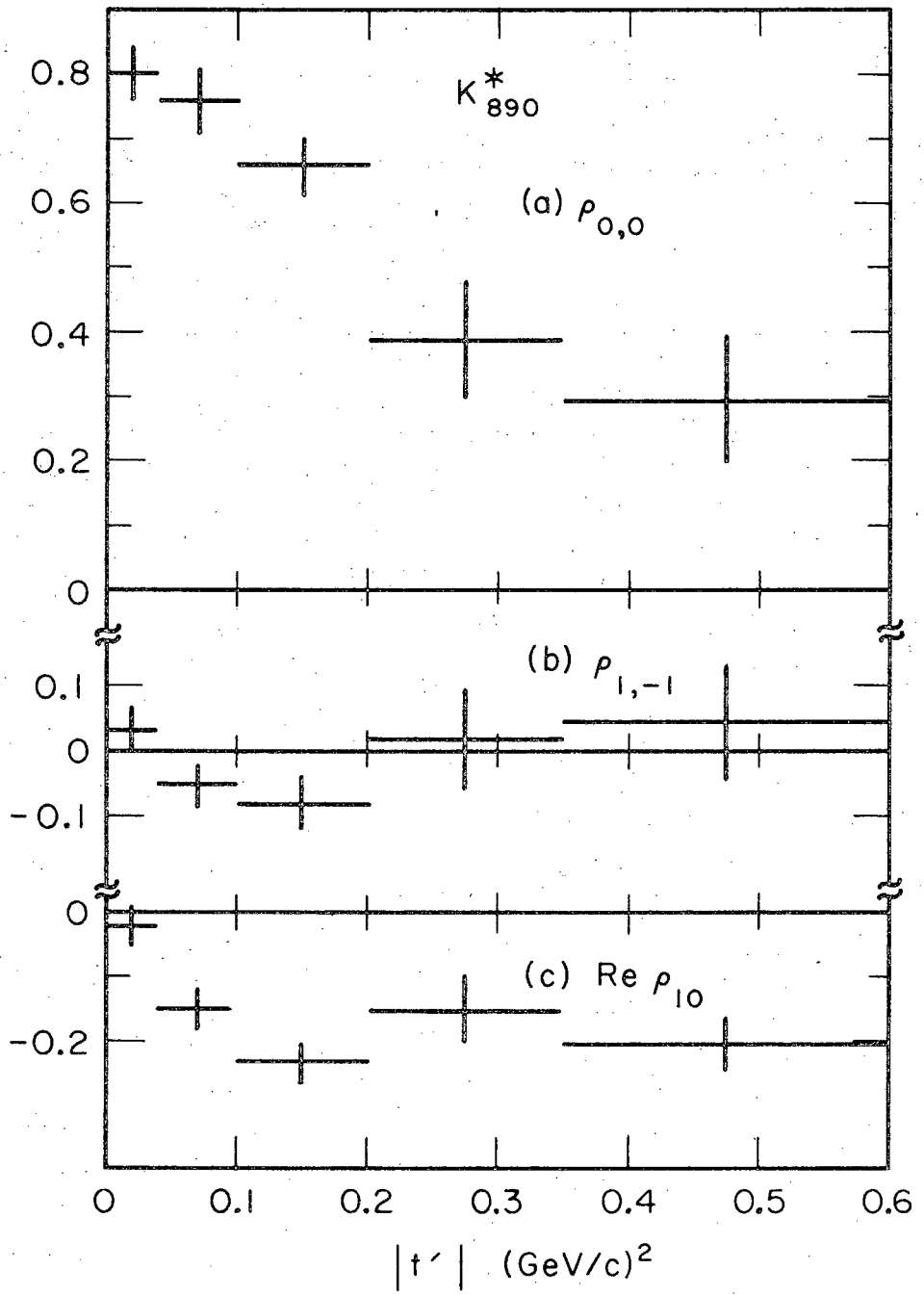
0.8
0.6
0.4
0.2
0
K^*_{890}
(a) $\rho_{0,0}$
0.1
0
-0.1
0
(b) $\rho_{1,-1}$
-0.2
(c) Re ρ_{10}
0
0.1
0.2
0.3
0.4
0.5
0.6
$|t'|$ (GeV/c)^2
XBL6910-3957

Fig. 12

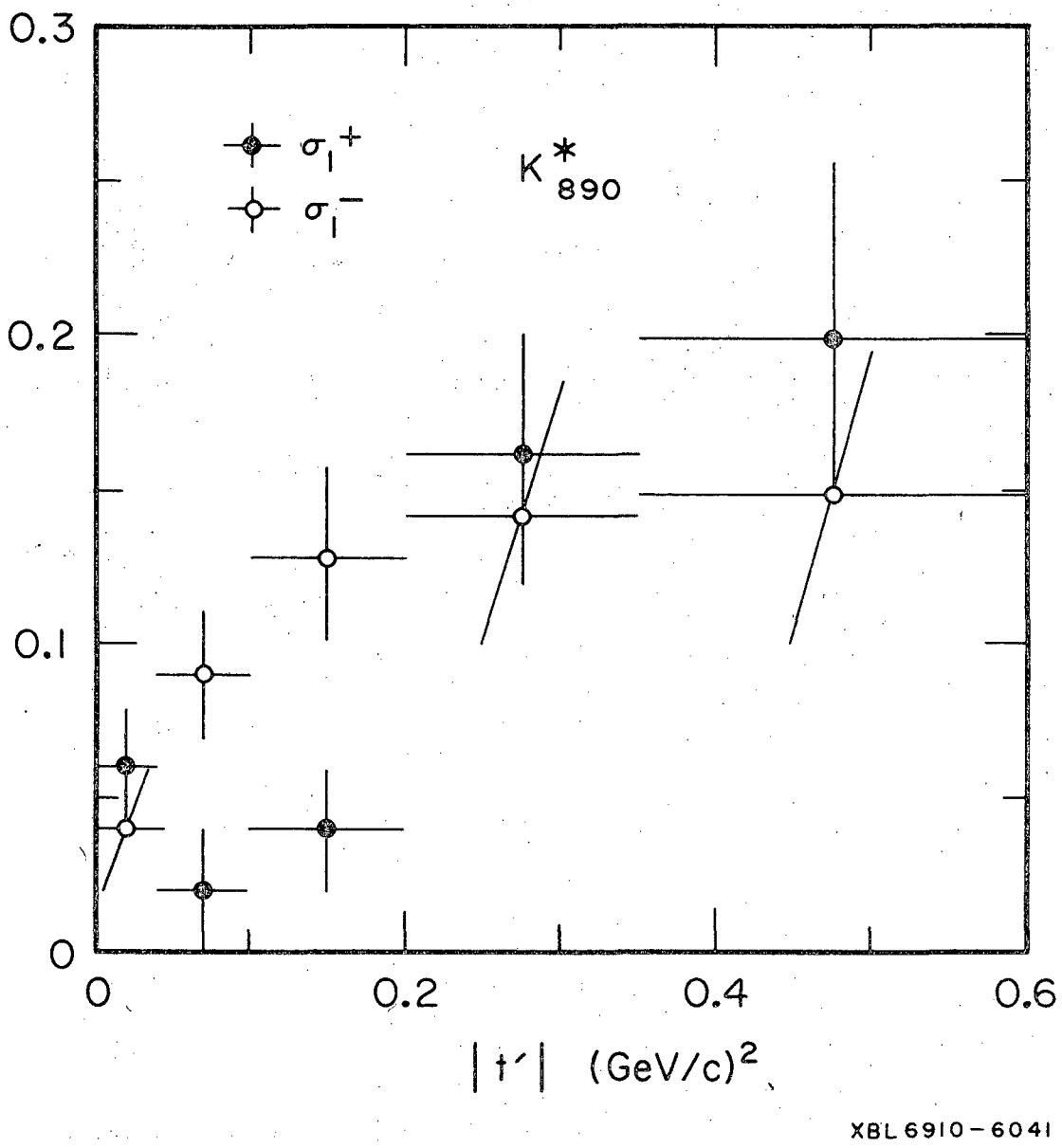

Fig. 13

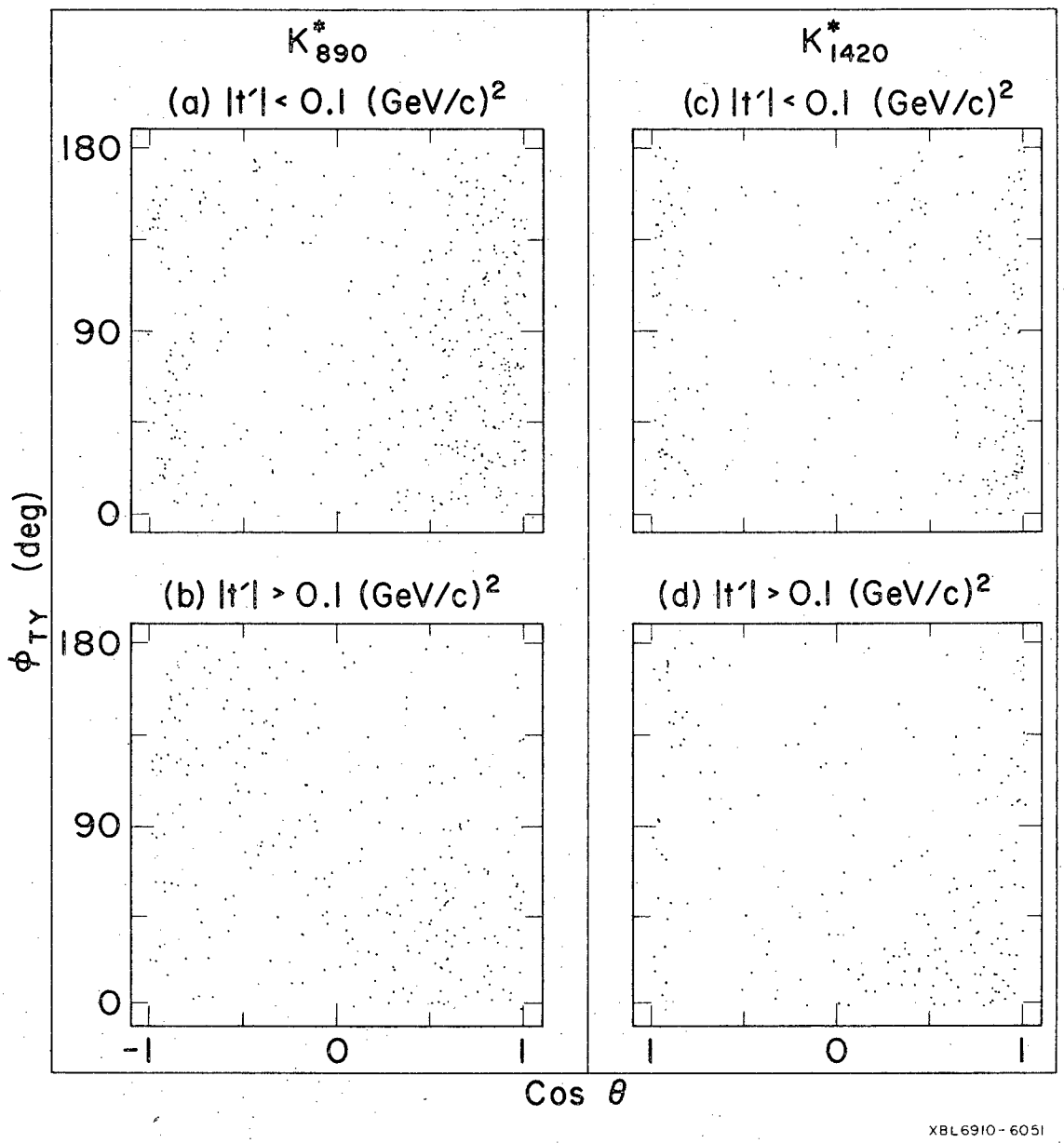
K^*_{890}
(a) $|t'| < 0.1$ (GeV/c)^2
K^*_{1420}
(c) $|t'| < 0.1$ (GeV/c)^2
(b) $|t'| > 0.1$ (GeV/c)^2
(d) $|t'| > 0.1$ (GeV/c)^2
ϕ_{TY} (deg)
180
90
0
-1
0
1
Cos θ
XBL6910-6051

Fig. 14

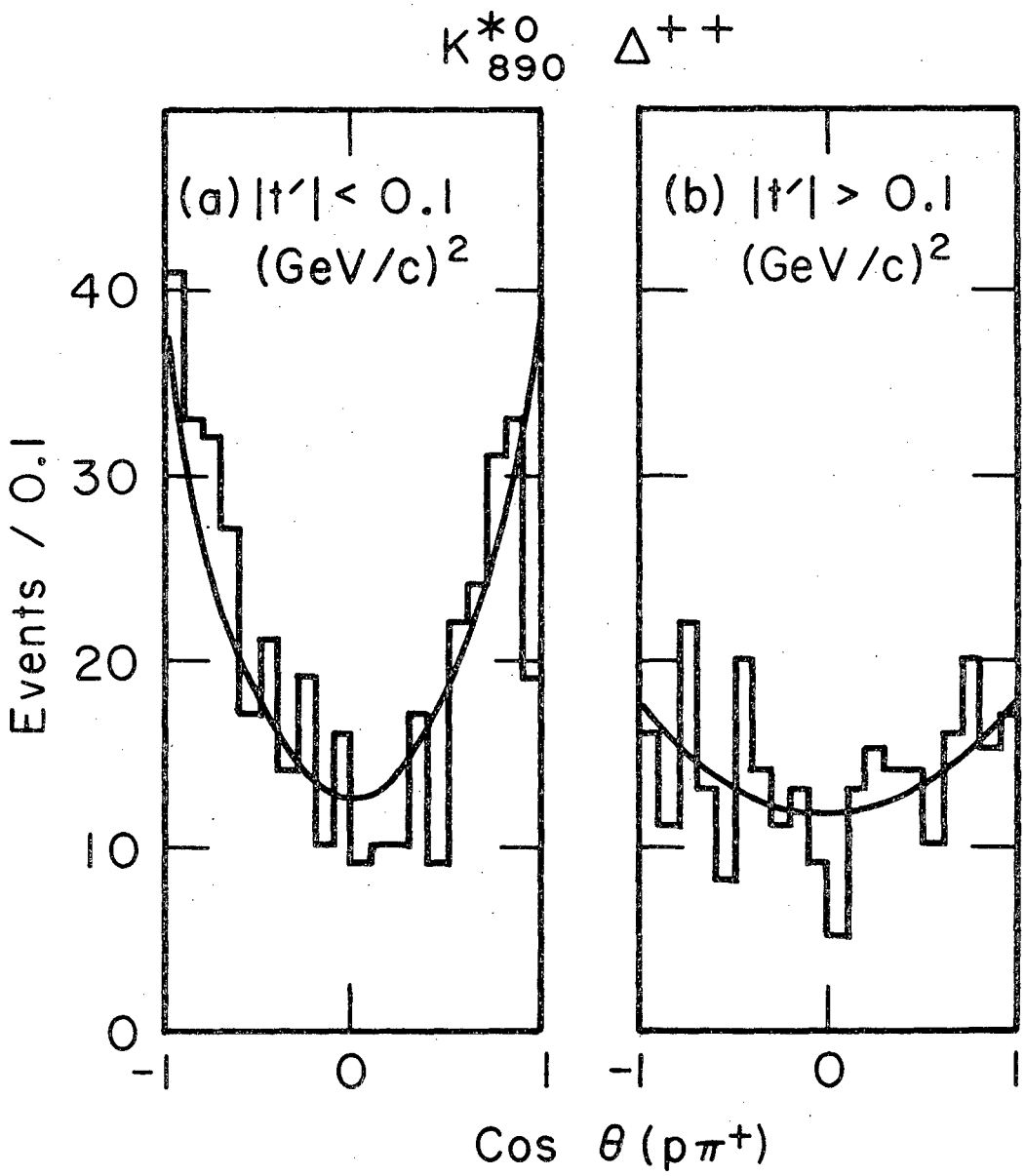
K^{*0}_{890} Δ^{++}
(a) $|t'| < 0.1$ $(GeV/c)^2$
(b) $|t'| > 0.1$ $(GeV/c)^2$
Events / 0.1
40
30
20
10
0
-1
0
1
Cos θ ($p\pi^+$)
XBL6910-6054

Fig. 15

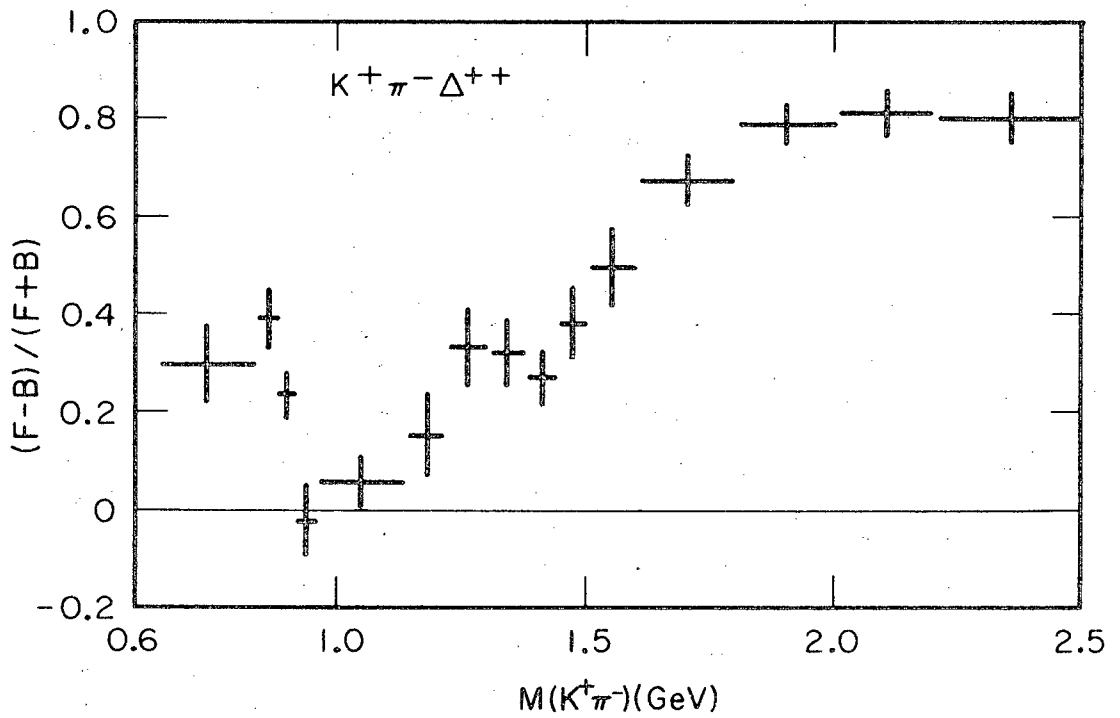
$K^+\pi^-\Delta^{++}$
(F-B)/(F+B)
1.0
0.8
0.6
0.4
0.2
0
-0.2
0.6
1.0
1.5
2.0
2.5
$M(K^+\pi^-)$(GeV)
XBL6910-6042

Fig. 16

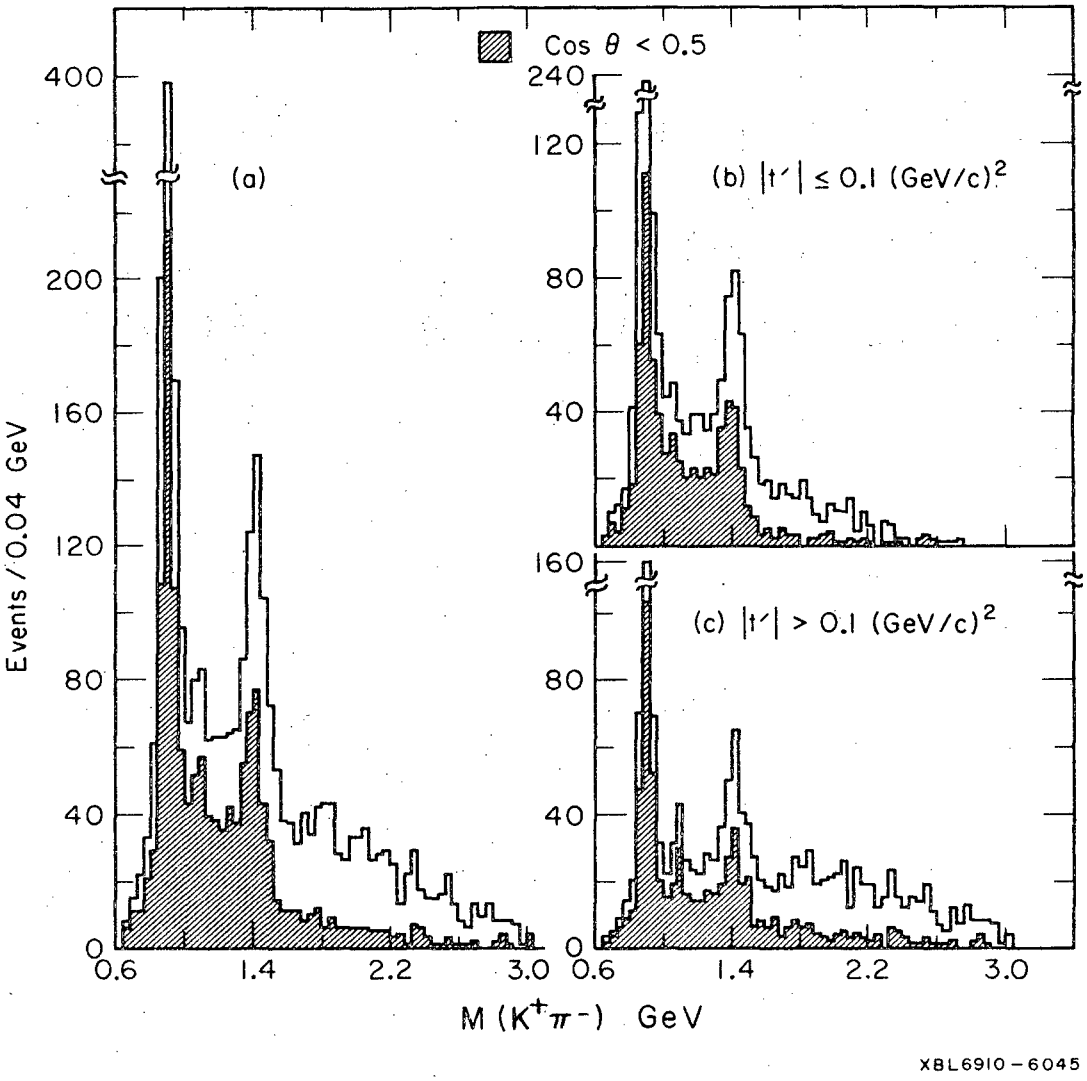
Cos θ < 0.5
(a)
(b) |t′| ≤ 0.1 (GeV/c)²
(c) |t′| > 0.1 (GeV/c)²
Events / 0.04 GeV
M (K⁺π⁻) GeV
XBL6910-6045

Fig. 17

TECHNICAL INFORMATION DIVISION
LAWRENCE RADIATION LABORATORY
UNIVERSITY OF CALIFORNIA
BERKELEY, CALIFORNIA 94720